Flexural performance of extruded ECC panel

Y.Y.Kim
Chungnam National University, Daejeon, Republic of Korea

B.Y.lee
University of Michigan, Ann Arbor, USA

B.-C. han
AMS Engineering, Daejeon, Republic of Korea

C.-G. Cho
Chosun University, Gwangju, Republic of Korea

ABSTRACT: This paper presents the materials, production process, and mix proportion applied to an extruded ECC panel and the effect of the fiber distribution characteristics, which are uniquely obtained with application of the extrusion process, on the flexural behavior of the panel. In order to demonstrate the fiber distribution effect, a series of experiments and analyses, including a sectional image analysis and micro-mechanical analysis, was performed. From test results, it was found that the flexural behavior of the panel was highly affected by slight variation in the mix composition. This is mainly attributable to the difference in mix composition resulting in change of the micro-mechanical properties as well as fiber distribution characteristics. In terms of the average fiber orientation, the fiber distribution was found to be similar to that derived under the assumption of a two-dimensional random distribution, irrespective of the mix composition. In contrast, the probability density function for the fiber orientation was measured to vary extensively depending on the mix composition.

1 INTRODUCTION

An Engineered Cementitious Composite (ECC) is a strain hardening cementitious composite that incorporates synthetic fibers and exhibits extreme tensile behavior. This behavior is mainly due to bridging of micro-cracks by the fibers and multiple cracking. (Leung 1996, Li & Leung 1992, Marshall & Cox 1988). The production methods of ECC include cast in place and spray. In addition to these methods, an extrusion process can be adopted. An extruded ECC panel is a precast composite fabricated by extrusion molding of cement, silica, sepiolite, natural minerals, and fibers to enhance flexural strength and stiffness. The application of extrusion molding to ECC enhances the strength, elastic modulus, and ductility of ECC. This stems from the lower porosity of extruded composites due to mechanical compaction, as well as to the aligned orientation of fibers. That, fibers aligned to the direction of the crack surface, which corresponds with that of extrusion, enhance crack resistance more than fibers oriented in two-dimensional random distributions. Shao & Shah (1997), Shao et al. (1995), Stang & Li (1999), Takashima et al. (2000), Akkaya et al. (2003) performed fundamental research for evaluating the mechanical properties of extruded ECC. However, there have been few studies on mix proportion, fiber orientation and dispersion, and the quantitative effect of the fiber distribution on the flexural behavior of an extruded ECC panel.

Therefore, this paper presents the materials, production process, and mix proportion applied to an extruded ECC panel and the effect of the fiber distribution characteristics on the flexural behavior of the panel. In order to evaluate the effect of the fiber distribution characteristics on the flexural behavior, an image processing technique was applied. Based on the results, the influence of the fiber distribution characteristics on the mechanical properties, represented here by flexural strength, was quantitatively evaluated.

2 EXTRUDED ECC PANEL

2.1 *Material*

Ordinary Portland cement with a density of 3.15 g/cm³ and ECC powder are used as binders. The ECC powder is composed of pulverulent materials

for strengthening the matrix and enhancing fire resistance. Silica powder with a density of 2.66 g/cm³ and a specific surface of 3.79 cm²/g and silica sand with a density of 2.64 g/cm³ and an average diameter of 0.2 mm are used as gravel. PVA fibers with diameter of 39μm and a length of 6~8 mm are used.

2.2 Production process

Figure 1 shows a diagram of the manufacturing procedure of the extruded ECC panel. The pulverulent material and fiber are mixed using an omni mixer and wet-mixing is then performed twice using a kneader mixer during a period of 3 minutes. Finally, extrusion is performed. The processing time is composed of dry-mixing for 4 minutes, wet-mixing for 6 minutes, and extrusion for 5 minutes. Figure 2 shows photographs of the manufacturing process of the extruded ECC panel, respectively.
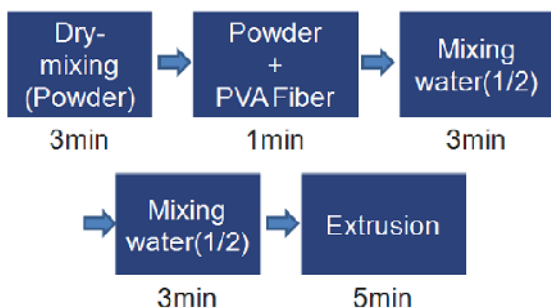
Figure 1. Mixing sequence of extruded ECC panel.

  (a) Dry mixing   (b) Extruding process of ECC panel
Figure 2. Production of extruded ECC panel.

2.3 Mix-proportion

A preliminary experiment was performed to determine the mix proportion with a water to binder ratio of 8~12%, a fly ash to binder ratio of 35%, and a silica to binder ratio of 50%. It is exhibited that it is hard to mix materials through inserting 0.5% PVA fiber. To prevent the clumping of fibers and to homogeneously disperse the fiber without increasing the water to binder water, an alternative mixing method (Section 2.2), is adopted and hydroxypropylmethyl-cellulose (HPMC, Atex Co., Korea) is inserted. Table 1 shows the 4 mix proportions employed to test the flexural behavior.

3 FLEXURAL PERFORMANCE

3.1 Specimens and experimental method

A four-point bending test was conducted to examine the performance of the extruded ECC panel. Figure 3 shows a specimen whose dimensions are 100×10×400 mm. Two specimens for each experi-

Table 1. Mixing properties of extrusion ECC panels.

Types	W/M* wt. %	OPC wt. %	ECC Powder† wt. %	Silica Powder wt. %	Silica Sand wt. %	SP wt. %	HPMC wt. %	PVA‡ vol.%
NO1	9.8	38	26	35.2	0	0.2	0.6	2
NO2	9.8	33	29	37.2	0	0.2	0.6	2
NO3	9.8	36	26	27.8	9.4	0.2	0.6	2
NO4	9.8	36	26	37.2	0	0.2	0.6	2

* M : Total weight of matrix
†ECC Powder : BFS, Sepiolite, Mg(OH)2, CaCO3, CSA, Al(OH)3, CW150
‡ Hydroxypropylmethyl-cellulose

mental variable were manufactured. The tests were carried out through displacement control using an actuator with a capacity of 250kN. The deflection at the center of the flexural specimens was measured by means of a LVDT installed at the center of the specimens. Figure 4 illustrates the flexural test apparatus. Flexural strength was calculated by Equation (5).

$$F_b = \frac{P \times l}{b \times d^2} \tag{5}$$

where is the flexural strength (MPa), is the maximum load (N), is the span length, and and are the width and height of the specimen, respectively.

3.2 Flexural behavior

Table 2 and Figure 4 present the flexural test results of the extruded ECC panel. The NO1 specimen exhibits approximately 50 MPa flexural strength, which is the maximum value among the fabricated extruded ECC panels, and brittle behavior (low tensile capacity), i.e. a drastic stress drop and low multiple cracking after first cracking due to high matrix strength. On the other hand, the other specimens exhibit strain hardening behavior after fiber cracking. The flexural strength of the NO2 and NO3 specimens is about 35~38 MPa, respectively, which is two to four times higher than that of general ECC (10 ~15 MPa). The ratio of deflection corresponding to the flexural strength and deflection at first cracking and the number of cracks in the NO3 specimens are 8.72~9.39 and 11~12, respectively. The NO3 specimens exhibit the maximum tensile capacity among the test specimens. The stiffness of the extru

ded ECC panel is measured to be 42.04~53.58 MPa and increases with increasing flexural strength.
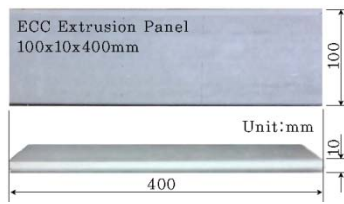
Figure 3. Specimen geometry.
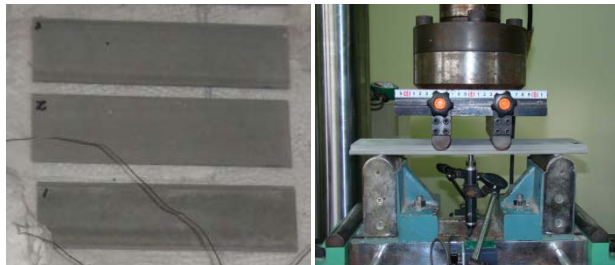
(a) Shape of specimens   (b) Test set-up

(c) Flexural behavior   (d) Crack distribution

Figure 4. Flexural test on extruded ECC panel.

Table 2. Test results of specimens.

Specimens	F_{bi} MPa	δ_{bi} mm	F_b MPa	δ_b mm	δ_b/δ_{bi}	Stiffness kN/mm
NO1	48.05	0.80	49.78	1.11	1.45	52.91
NO2	29.04	0.68	37.01	6.11	9.06	42.14
NO3	31.43	0.69	36.22	2.25	3.26	47.79
NO4	32.97	0.77	37.07	4.50	5.95	46.82

F_{bi} : Flexural strength at initial crack
δ_{bi} : Mid-span deflection at F_{bi}
F_b : Maximum flexural strength
δ_b : Mid-span deflection at F_b
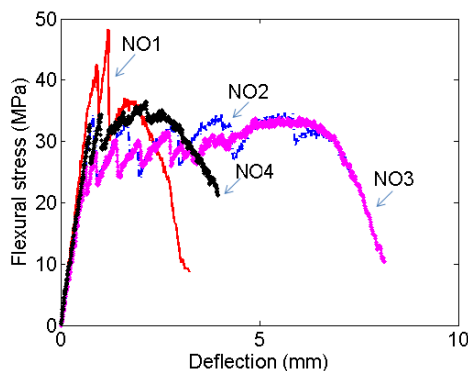
Figure 4. Flexural behaviors of ECC-extrusion panels.

4 FIBER DISTRIBUTION

4.1 *Fiber detection in fiber image*

The distribution characteristics of fiber can be quantitatively represented by detecting the fibers in a fiber image and calculating the distribution coefficient by mathematical treatment. In this study, an enhanced evaluation technique for PVA fiber dispersions in engineered cementitious composites is adopted (Lee et al. 2009). This technique is essentially composed of stepwise tasks. First, the specimen is prepared and treated, followed by acquisition of a fluorescence image using a fluorescence microscope with a CCD (charged couple device). Based on the proposed image processing algorithm, the fiber images are then automatically detected in a binary image, which is originally converted from the fluorescence image. Next, a mathematical treatment is performed on the data obtained from the previous task, which finally provides the calculated fiber dispersion coefficient of the composite.

The image processing technique for detecting fibers is composed of two tasks. First, the fiber images detected by a prototype thresholding algorithm are classified into five types by a watershed segmentation algorithm (Vincent & Soille 1991) and an artificial neural network. Next, aggregate fiber images, that is, misdetected fiber images, are detected correctly by means of the watershed segmentation algorithm and morphological reconstruction (Vincent 1993).

4.2 *Fiber distribution coefficient*

The degree of fiber dispersion is quantitatively evaluated based on calculation of the coefficient, referred to as the fiber dispersion coefficient, as expressed by Equation (6).

$$\alpha_f = \exp\left[-\sqrt{\frac{\sum(x_i-1)^2}{n}}\right] \qquad (6)$$

where n is the total number of fibers on the image and x_i denotes the number of fibers in the i-th unit, which is a square portion allocated to the i-th fiber on the assumption that the fiber dispersion is perfectly homogeneous. The value for tends to 1 for a homogeneous dispersion of fibers, or 0 for a severely biased dispersion.

The second distribution characteristic is the distribution of the fiber orientation. The inclined angle of the fiber to the cutting plane can be calculated by Equation (7).

$$\theta = \cos^{-1}\left(\frac{l_s}{l_l}\right) \qquad (7)$$

where and are the shortest diameter and longest diameter of the fiber image in sectional image, respectively.

4.3 *Fiber distribution*

Table 3 shows the distribution coefficient analyzed according to the specimens by adopting the image processing described in section 4.1 & 4.2. The fiber images were taken in three random positions with a size of 8×8 mm^2. Figure 5 shows fiber images of the NO1, NO2, NO3 and NO4 specimens, which exhibit the maximum difference in flexural behavior. The fibers in the NO3 specimen are more uniformly dispersed in the cross section compared to the others and the NO2, NO4, and NO1 specimens display the

Table 3. Test results of specimens.

Specimens	α_f	θ (°)
NO1	0.27±0.037	45±1.3
NO2	0.31±0.045	44±2.2
NO3	0.28±0.048	45±2.0
NO4	0.30±0.041	44±1.4
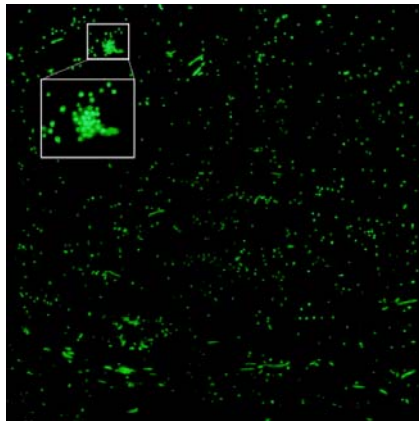
(a) NO1
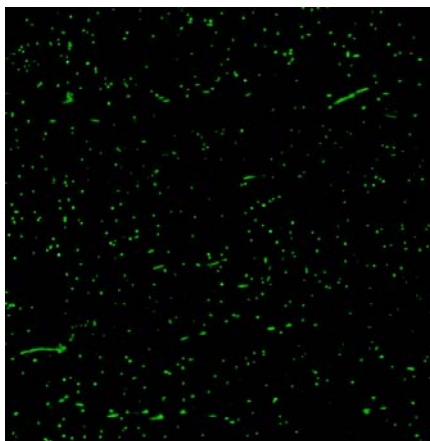
(b) NO4

Figure 5. Typical fiber images.

largest fiber dispersion coefficients in the given order, as shown in Table 3 and Figure 6. Torigoe et al. reported that the tensile capacity of ECC increases as the fiber dispersion is increased (Torigoe et al. 2003). Therefore, it can be predicted that the tensile capacity increases in the order of NO3, NO2, NO4, and NO1 and flexural test results exhibited corresponding results (Fig. 4).

There is no significant difference in the fiber orientation according to the specimens. The average fiber orientation of the NO2 and NO3 specimens is about $38°$. On the other hand, the average fiber orientation of the NO1 and NO4 specimens is about $41°$. If the fiber orientation is assumed to have a three-dimensional random distribution, then the fiber orientation is $57.3°$. If the fiber orientation is assumed to have a two-dimensional random distribution, then the fiber orientation is $45°$. Therefore, fibers of extruded ECC are aligned more than that obtained by assuming a two-dimensional random distribution through extrusion process.

Figure 6 shows the probability density function for the fiber orientation according to the specimens. As can be seen in the figure, the probability density functions measured by the image analysis are considerably different from those obtained by assuming two- or three-dimensional random distributions for the fiber orientation.

5 CORRELATION BETWEEN FLEXURAL BEHAVIOR AND FIBER DISTRIBUTION

The flexural behavior and fiber distribution characteristics of extruded ECC vary according to the mix proportion. In this study, it is assumed that difference in the mix proportion leads to the difference in fiber distribution, which is the primary factor for the flexural behavior of extruded ECC, and the test results were analyzed on the basis of this assumption. Figure 7 shows the fiber bridging curves obtained on the basis of the probability density function for the fiber orientation shown in Figure 6. The frictional bond strength was assumed to be 2.9 MPa on the basis of experimental results reported by Kim et al. (2007). The chemical bond strength was also assumed to be 1.85 J/m^2 on the basis of experimental results obtained by Li et al. (2002).

The behavior of ECC is governed by the fracture toughness of the matrix (J_{tip}), the strength of the matrix (f_t), and the fiber bridging characteristics. The potential of pseudo strain hardening behavior increases with decreasing fracture toughness and matrix strength and increasing peak bridging stress. J_{tip} of the NO1 specimens is higher than that of other specimens, because the water to binder ratio of these specimens is lower than that of the other spe-

cimens. In particular, J_{tip} of the NO1 specimens is 94.3 % higher than that of the NO3 specimens when

(a) NO1

(b) NO4

(c) NO2

(d) NO3
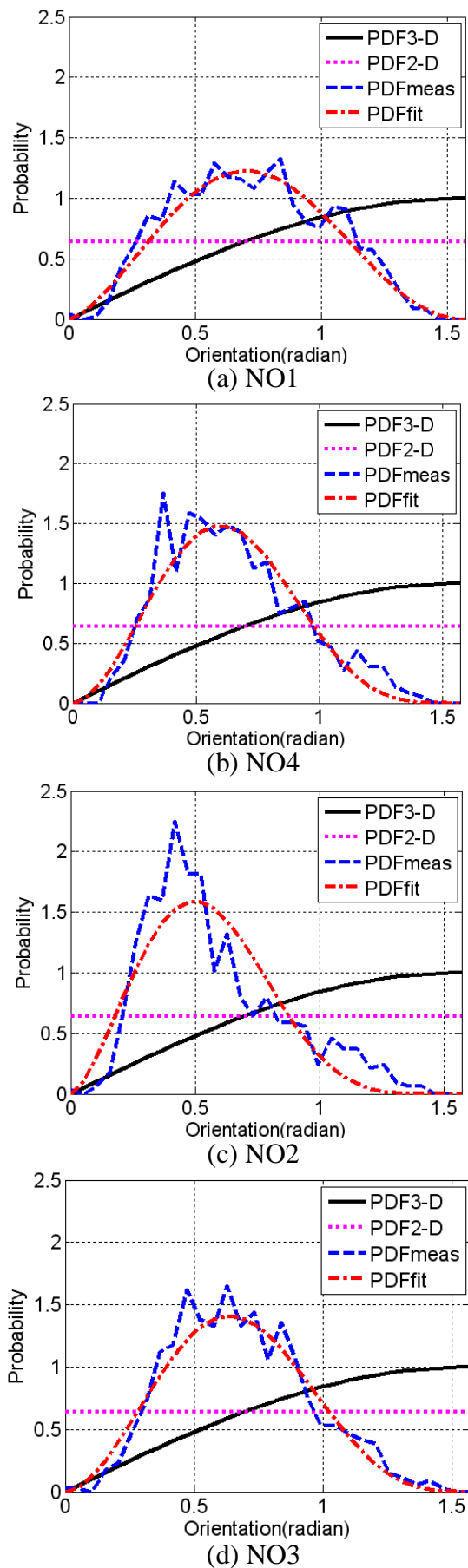
Figure 6. Typical probability density function of fiber orientation.

J_{tip} is calculated indirectly on the basis of F_{bi}, which leads lower potential for pseudo strain-hardening behavior (Kim et al. 2007). The fiber dispersion coefficient of the NO1 specimens is about 14% lower than that of the NO3 specimens. of specimens are 70.6, 99.3, 119, and 89.5 J/m^2, respectively. σ_0 of specimens are 5.11, 5.44, 5.67, and, 5.33 MPa, respectively.

As shown in Figure 7, the NO1 specimens exhibit the lowest J_b' and σ_0, which are 40.9 % and 9.98% lower than those of the NO3 specimens, respectively, and lead to the lowest flexural tension capacity. J_{tip} of the NO4 specimens, which incorporated silica sand with large diameter, is 14.1 % higher than that of the NO3 specimens when J_{tip} is calculated indirectly on the basis of F_{bi}, which leads lower potential for pseudo strain-hardening behavior. The fiber dispersion coefficient of the NO4 specimens is about 11.0% lower than that of the NO3 specimens. Owing to these two phenomena, the flexural tension capacity of the NO4 specimens is lower than that of the NO2 and NO3 specimens.

When J_{tip} is assumed to be 10 J/m^2, which is calculated on the basis of a reference paper (Lee 2009), the toughness ratio (J_b'/J_{tip}) according to four mix proportions are 7.06, 9.93, 11.9, and 8.95, respectively. It is assumed that the fracture toughness of the matrix is linearly relation with the strength of the matrix, because the matrix used in ECC shows linear elastic behavior compared with the concrete. Therefore, the fracture toughness at the crack tip of extruded ECC is increased about nine-fold relative to that of general ECC, because the flexural strength of extruded ECC is three times greater than that of general ECC.

The potential for pseudo strain-hardening behavior of the NO2 and NO3 specimens is greater than that of the NO1 and NO4 specimens, which is attributed to the good fiber dispersion and high J_b' and σ_0 of the NO2 and NO3 specimens. The tensile capacity of the NO3 specimens is higher than that of the NO2 specimens with the same water to matrix and water to binder ratios. This could more readily be explained on the basis of the fiber dispersion of the NO3 specimens being about 6.3% higher than that of the NO2 specimens. Therefore, it is confirmed that the flexural behavior of the extruded ECC panel is affected by the fiber distribution.
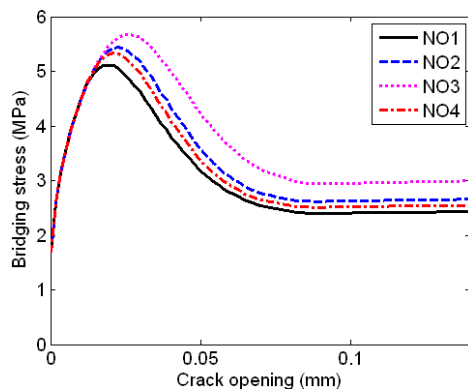
Figure 7. Comparison of representative fiber bridging curves.

6 CONCLUSIONS

This paper presents a theoretical and experimental study on the manufacture of an extruded ECC panel, which exhibits multiple cracking and potential pseudo strain-hardening behavior, and the effect of fiber distribution characteristics on the flexural behavior of the panel. The following conclusions have been drawn: (1) The extruded ECC, which exhibits pseudo strain-hardening behavior, can be made with dry mixing of materials and 2% PVA fiber, wet-mixing, and extrusion. The extruded ECC panel exhibits maximum tensile capacity when the water to matrix is 9.8% and the ratios of cement, ECC powder, and silica sand are 33, 29 37.2, respectively. The stiffness of the extruded ECC panel increases with increasing flexural strength; (2) The fiber dispersion is found to be better with increasing flexural tensile capacity. The average fiber orientation of the specimens is about 44°. If the fiber orientation is assumed to have two- and three-dimensional random distributions, then the fiber orientation is 45° and 57.3°, respectively. In terms of the average fiber orientation, the fiber distribution was found to be similar to that given with the assumption of a two-dimensional random distribution. The probability density functions measured by the image analysis are considerably different from those obtained by assuming two- or three-dimensional random distributions for the fiber orientation; and (3) the fiber distribution varies according to the mix proportion with same extrusion process, which leads to differences in the flexural behavior. Therefore, it is necessary to consider the mix proportion and the resultant fiber distribution as well as the manufacturing process to achieve desired performance such as flexural strength and tensile capacity.

ACKNOWLEDGEMENTS

REFERENCES

Akkaya, Y, Peled, A, Shah, SP 2000. Parameters related to fiber and processing in cementitious composites.*Mater Struct* 33:515–24.

Kim JK, Kim JS, Ha GJ, and Kim YY 2007. Tensile and Fiber Dispersion Performance of ECC Produced with Ground Granulated Blast Furnace Slag. *Cement and Concrete Research* 37(7):1096-1105.

Lee BY 2009. Fiber Distribution Evaluation Using Digital Image Processing and Its Effect on Tensile Behavior of Fiber Reinforced Cement composites. Doctoral thesis, KAIST.

Lee BY, Kim JK, Kim JS, and Kim YY 2009. Quantitative Evaluation Technique of PVA (Polyvinyl Alcohol) Fiber Dispersion in Engineered Cementitious Composites. Cem Concr Compos.31(6):408-417.

Leung, CKY 1996. Design criteria for pseudoductile fiber-reinforced composites. *ASCE J Engrg Mech.*122(1):10-14.

Li, VC & Leung, KY 1992. Steady-state and multiple cracking of short random fiber composites. *ASCE J Engrg Mech.*118(11):2246-2264.

Li VC, Wu C, Wang S, Ogawa A, and Saito T 2002. Interface Tailoring for Strain-hardening PVA-ECC. *ACI Materials Journal.*99(5):463-472.

Marshall, DB and Cox, BN 1988. A J-integral method for calculating steady-state matrix cracking stressed in composites. *Mechanics of Materials* 7(2):127-133.

Shao, Y & Shah, SP 1997. Mechanical Properties of PVA Fiber Reinforced Cement Composites Fabricated by Extrusion Processing. *ACI Materials Journal* 94(6):555-564.

Shao, Y, Markunte, S, Shah, SP 1995 Extruded fiber-reinforced composites. *Concr Int* April:48–52.

Stang, H & Li, VC 1999. Extrusion of ECC-Material, in Proc. of High Performance Fiber Reinforced Cement Composites 3(HPFRCC 3), Ed. Reinhardt and A. Naaman, Chapman & Hull, pp.203-212

Takashima H, Miyagai K, Hashida T, Li VC 2003. A design approach for the mechanical properties of polypropylene discontinuous fiber reinforced cementitious composites by extrusion molding, *Engineering Fracture Mechanics* 70:853-870.

Torigoe S, Horikoshi T, and Ogawa A 2003 Study on evaluation method for PVA fiber distribution in engineered cementitious composite. *Journal of Advanced Concrete Technology* 1(3):265-268.

Vincent L 1993. Morphological Grayscale Reconstruction in Image Analysis: Applications and Efficient Algorithms. *IEEE Transactions on Image Processing* 2(2):176-201.

Vincent L & Soille P 1991. Watesheds in digital spaces: An efficient algorithm based on immersion simulations. *IEEE Transactions on Pattern Analysis and Machine Intelligence.* 13(6): 583-598.